RSC Advances

PAPER

View Article Online
View Journal | View Issue

Cite this: *RSC Adv.*, 2026, **16**, 14199

Artificial neural network model of the capacity of diethylenetriamine functionalised zinc oxide-apricot stone shell nanocomposite for sequestering 2,4-dichlorophenoxyacetic acid from wastewater

Akinshola Olabamiji Akinola, Eswaran Prabakaran, Krishna Govender and Kriveshini Pillay *

A novel nanocomposite, diethylenetriamine functionalised zinc oxide-apricot stone shell (ZnO@Ap/DETA), has been synthesised for the efficient sequestration of 2,4-dichlorophenoxyacetic acid (2,4-D). The capacity and removal efficiency were evaluated using an artificial neural network (ANN). The characterisation of ZnO@Ap/DETA was performed to determine its physicochemical properties through various instrumental techniques. The nanocomposite displayed a more uniform mesoporous structure, having pores with an average size of 34.065 nm and a significantly enhanced surface area of 26.56 m^2 g^{-1}, approximately 13 times greater than that of the pristine apricot stone (AP) shells (2.076 m^2 g^{-1}). ZnO@Ap/DETA was utilised to adsorb 2,4-D from synthetic wastewater at pH 3, 50 mg adsorbent dose and 30 mg L^{-1} initial 2,4-D concentration, and a real wastewater sample at 18.5 mg L^{-1} 2,4-D concentration and 50 mg adsorbent dose, achieving performance efficiencies of 98.6% and 85.41%, respectively, after a 90-minute agitation period at 25 °C. The data on adsorption were consistent with the pseudo-second-order kinetic model and Langmuir isotherm, and thermodynamic investigations suggested that the process was spontaneous, favourable, and exothermic, as evidenced by a $\Delta H°$ value of −92.85 KJ mol^{-1}. To optimise the adsorption process, an ANN model was developed, comprising five input parameters, two hidden layers, and two output parameters. The developed model successfully predicted 2,4-D removal efficiency with a mean absolute error (MAE) of 0.2952, a mean squared error (MSE) of 0.4227, and a high R^2 of 0.9991. These results highlight the potential of ZnO@Ap/DETA for environmental remediation and for wastewater treatment.

Received 20th January 2026
Accepted 5th March 2026

DOI: 10.1039/d6ra00502k

rsc.li/rsc-advances

1 Introduction

The escalating utilisation of pesticides presents a huge danger to water quality because of the potential contamination from these substances. Such compounds can lead to detrimental environmental effects. 2,4-Dichlorophenoxyacetic acid (2,4-D) represents one among the most popularly utilised herbicides globally, employed for the management of both terrestrial and aquatic weed species.[1] Its extensive distribution has led to the detection of 2,4-D in significant waterways across urban areas in the United States[2] and, for the first time, Horn and colleagues[3] determined levels of 2,4-D in bodies of water in South Africa in amounts that even surpassed the drinking water standards in Europe. The prevalence of this chemical was widespread; 74% of examined soil samples in South Africa attested to the presence of the chemical.[4] Its application in both water and land farming procedures causes concern about whether 2,4-D pollutes water bodies or not, putting the already existing species and communities that depend on the source of water to sustain their survival at risk. The primary pathways through which this herbicide contaminates surface water include the disposal of wastewater from manufacturing facilities, accidental spills during transport, runoff, and leaching from agricultural and grassland regions. Notably, the concentration of 2,4-D in water bodies tends to peak during the crop cultivation season, a period characterised by heightened application rates.[5] Reported concentrations of 2,4-D in aquatic environments have reached levels between 359 μg L^{-1} and 636 μg L^{-1}, significantly exceeding the lethal dose thresholds established for various aquatic organisms.[6,7] In proximity to agricultural fields, concentrations can soar to as high as 4 mg L^{-1}, far surpassing the WHO's permissible limit of 0.02 mg L^{-1} for drinking water.[5] As a toxic pollutant, 2,4-D exhibits poor biodegradability.[8] The contamination of groundwater has emerged as a significant concern, adversely affecting the quality of drinking water worldwide. When living organisms are exposed to 2,4-D, it can

Department of Chemical Sciences, University of Johannesburg, South Africa. E-mail: akinsholaakinola@gmail.com; eprabachemistry86@gmail.com; krishnag@uj.ac.za; kriveshinip@uj.ac.za

cause significant ecological repercussions, including mortality rates among both plant and fish populations, contamination of potable water sources, and bioaccumulation within various ecosystems. The presence of 2,4-D in aquatic environments presents substantial health hazards for both people and animals because of its poisonous and mutagenic qualities. This exposure correlates with a range of health complications, including congenital anomalies, respiratory disorders, renal diseases, and disturbances in urinary and endocrine functioning.[9] This issue poses a substantial challenge to achieving the sixth sustainable development target, which aspires to ensure that everyone has access to clean water and sanitary facilities by 2030. As a result, it is important to implement effective wastewater treatment processes to comply with established safety regulations prior to discharge into aquatic ecosystems.

Methods that include nanofiltration, photocatalysis, electrocoagulation, photo–Fenton processes, biological treatments, ultrasound application, sedimentation, and adsorption have been extensively acknowledged for their efficacy in the remediation of contaminated water containing pesticides.[1,10] Among these methods of water treatment, adsorption stands out because of its significant advantages such as minimal energy usage, selectivity, and accessibility to a wide array of adsorbents, which enables effective treatment while minimising harmful by-products.[11] It is a budget-friendly technique. Activated carbon (AC), which is widely available, has been successful in eliminating numerous contaminants from water, thanks to its adsorption capabilities.[12] Nevertheless, the high expense associated with AC limits its feasibility for large-scale industrial use, prompting the investigation of more economical, renewable, and efficient alternative adsorbents for water and wastewater treatment.[13] This leads to an ongoing effort which exists to identify more affordable adsorbents.

The removal of 2,4-D from water-based solutions has been successfully accomplished by utilising a range of agricultural by-products and natural substances, including *Balanites aegyptiaca* seed shell,[1] fly ash zeolites,[9] chest nutshell,[14] rice husk,[15] orange peel, millet waste, apple shell, banana peel,[16] wheat straw,[17] raw peach and apricot shell,[18] coffee wastes,[19] cotton plant ash, corncob biochar,[20] watermelon peel hydrochar[21] and groundnut shell.[22]

Apricot, classified within the Rosaceae family, is predominantly cultivated across the regions of Africa, Asia, and Europe. During the processing of apricot seeds, a significant quantity of shells is generated, which are typically discarded as agricultural waste or utilised as a supplement to enhance soil fertility.[23] The by-products of apricot have been recognised as a cost-effective adsorbents for sequestering dyes, pesticides, and heavy metals.[18,24,25] However, the potential of apricot stone shells for sequestering 2,4-D herbicide remains inadequately investigated. The application of unmodified adsorbents frequently results in below-average performance, attributed to restrictions in the capacity and efficiency of adsorption. This limitation is corroborated by findings in prior research.[18]

Apricot shell alone tends to adsorb a broad spectrum of contaminants non-specifically, and repeated usage may lead to structural degradation.[26,27] In contrast, ZnO nanoparticles alone demonstrate considerable adsorption capabilities, but their tendency to agglomerate reduces their effective surface area. The recovery of pure ZnO after adsorption poses challenges, while apricot shells may face issues related to pore blockage. The incorporation of ZnO nanoparticles enhances the structural integrity of the apricot shell matrix, thereby improving its mechanical stability and reusability. Furthermore, the presence of ZnO promotes selective adsorption mechanisms that target specific pollutants, such as 2,4-D. The dispersion of ZnO within the apricot shell matrix reduces aggregation, thus increasing surface accessibility for adsorption. This composite structure allows for more efficient regeneration through washing or thermal treatment methods, thereby preserving performance integrity. Unlike the individual components of a pristine apricot shell or ZnO, the composite would demonstrate stability across multiple adsorption–desorption cycles.[28] The modification of the ZnO@Ap composite with DETA introduces additional active sites (amine groups), which enhances the interaction capabilities between the adsorbent and the target pollutants. This composite synergistically combines the high surface area and porosity of apricot shell with the reactive sites provided by ZnO and DETA, resulting in superior adsorption efficiency for herbicides compared to the individual components.[29,30] The composite would effectively optimise the strengths of its constituents, leading to improved contaminant removal efficiency and a reduction in the overall costs associated with wastewater treatment compared to more expensive adsorbents.[31]

The increasing global emphasis on environmental protection, coupled with advancements in pollution control technologies, has led to stricter regulatory standards for pollutant discharge. In order to ensure compliance with these regulations, it is essential to explore and optimise innovative operational and design approaches for wastewater treatment.[11] A critical aspect of this optimisation involves the accurate modelling of adsorption processes, which provides valuable insights into system performance, process control, and long-term monitoring strategies. Among various modelling techniques, artificial neural networks (ANNs) have emerged as an effective instrument due to their ability to analyse complex adsorption data and identify non-linear relationships between variables. Unlike conventional models, ANNs are data-driven and do not require predefined assumptions about underlying adsorption mechanisms, making them highly adaptable to dynamic environmental conditions.[32]

Previous studies have successfully employed ANNs to predict adsorption efficiencies in various systems, including copper(II) removal using pumice,[33] basic yellow dye decolourisation *via* electrocoagulation,[34] Congo red dye elimination using cetyltrimethylammonium bromide-modified magnetic apricot shells,[24] and lead(II) extraction with rice husk.[35] The ANN model has been used for Pb^{2+} removal with *Prosopis juliflora*-based adsorbents.[36] Despite these advancements in the past few years, no findings have yet explored the application of ANNs for modelling the adsorption capacity of 2,4-D removal using diethylenetriamine-functionalised zinc oxide–apricot shell

nanocomposites. In a bid to address this research gap, the present study focuses on synthesising a novel, environmentally benign adsorbent composed of diethylenetriamine-functionalised zinc oxide supported on apricot shell (ZnO@Ap/DETA). This composite was designed to enhance 2,4-D adsorption through an expanded surface area as well as improved active sites. The adsorption performance was systematically evaluated by optimising key operational parameters, including the pH of the solution, the dosage of the adsorbent, the duration of contact, and the initial concentration of 2,4-D. Furthermore, the study investigated the kinetics and thermodynamics of adsorption which clarify the fundamental principles involved while also assessing the reusability of the composite over multiple adsorption–desorption cycles. The adsorption efficiency and capacity were modelled using Python-based artificial neural networks to enhance predictive accuracy. Finally, the practical applicability of the ZnO@Ap/DETA composite was tested using real wastewater samples spiked with 2,4-D, providing insights into its potential for large-scale implementation.

2 Materials and methods

2.1 Materials

High-quality analytical reagents were obtained from Sigma-Aldrich and Sisco Research Laboratories Pvt. Ltd for use in this study. The chemicals included sodium hydroxide (NaOH) with a purity greater than 98%, $Zn(NO_3)_2 \cdot 6H_2O$ (zinc nitrate hexahydrate) at 99% purity, diethylenetriamine (DETA) with 99% purity, and 2,4-D at 97% purity. AP shells were sourced from the Johannesburg Fresh Produce Market in City Deep, South Africa. After collection, the shells were dried at 105 °C for 24 h, ground into particles sized between 10 and 75 μm, and preserved for future use in the composite synthesis.

2.2 Synthesis of ZnO@Ap nanocomposite

The ZnO@Ap nanocomposite was prepared by a hydrothermal method, in which 8.0 g of $Zn(NO_3)_2 \cdot 6H_2O$ was dissolved in 500 ml of deionised water and homogenised by stirring for 10 minutes. Then, 10 g of the Ap powder was incorporated into the solution under continuous agitation for 50 minutes. This was followed by pH adjustment to 9.5 using 0.1 M aqueous NaOH. This was stirred for another 60 minutes, then heated to 180 °C for six hours in an autoclave. Deionised water and ethanol were used to rinse the cooled resulting product, which was then centrifuged and dried for 24 hours at 60 °C. The nanocomposite was then calcined at 200 °C for 4 hours under an air atmosphere for mild post-curing in order to aid solvent removal and purification as well as surface stabilisation and enhancement of oxygen-containing functional groups, without disrupting the structural integrity of the ZnO@Ap composite. The schematic diagram of ZnO@Ap nanocomposite preparation is shown in Scheme 1.

2.3 Modification of ZnO@Ap nanocomposites with DETA

The DETA solution was formed by putting 2 ml of 99% in 100 ml of ethanol. Then, 5.0 g of the ZnO@Ap was introduced to this solution and agitated for six hours at 60 °C. These conditions were chosen based on preliminary optimisation and chemical considerations to provide a balance between the efficiency of functionalisation, pore structure preservation, and adsorption efficiency. The modified adsorbent was allowed to cool down to room temperature, washed with ethanol and dried at 60 °C for 24 hours. The modified nanocomposite was stored for

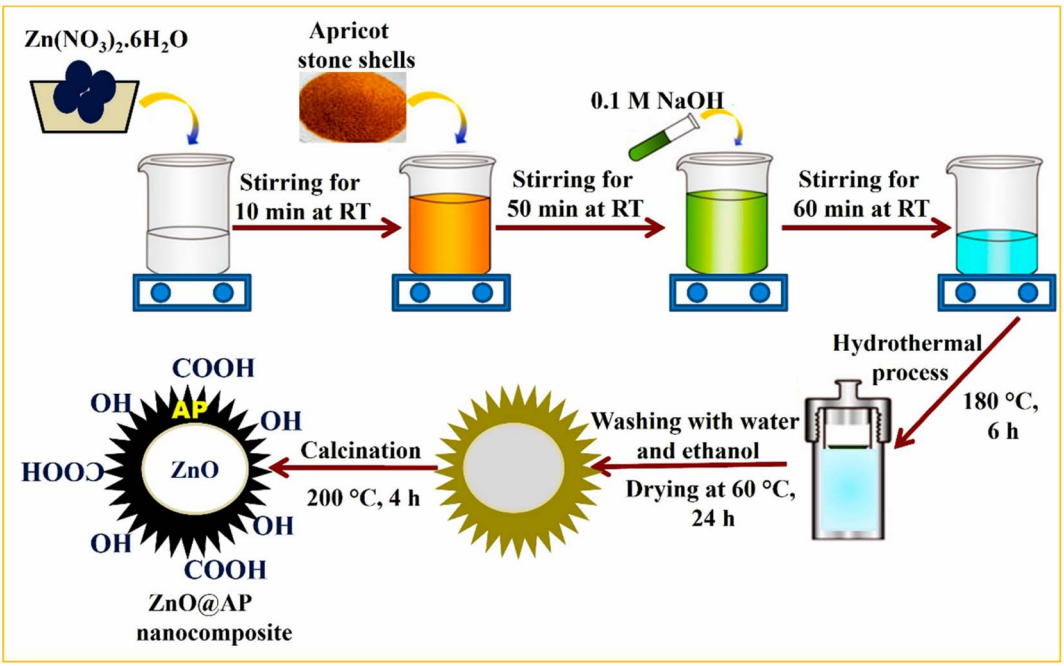

Scheme 1 Representation of the fabrication of ZnO@Ap nanocomposite using the hydrothermal process.

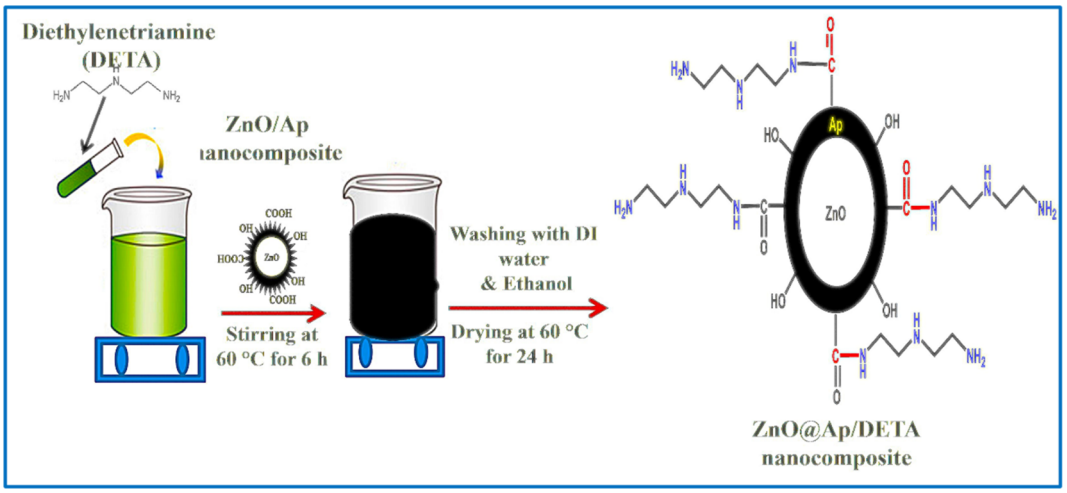

Scheme 2 The schematic illustration of modified ZnO@Ap/DETA nanocomposite.

characterisation and application. The schematic diagram of the modified ZnO@Ap/DETA nanocomposite is found in Scheme 2.

2.4 Characterisation of ZnO@Ap/DETA nanocomposites

The ZnO@Ap/DETA nanocomposite was analysed using multiple advanced characterisation techniques. Both the untreated AP and the prepared ZnO@Ap/DETA were evaluated. Brunauer–Emmett–Teller (BET) adsorption/desorption isotherm analysis was carried out on a ASAP-2020 (micromeritics) equipped with TriStar II Plus 3.00, 456. The specific surface area was determined using nitrogen at −196 ± 1 °C. Degassing was done at 170 °C for 5 hours. The Barrett–Joyner–Halenda (BJH) method was employed for the pore size analysis from the nitrogen desorption isotherm. The scanning electron microscopy (SEM) and energy dispersive X-ray spectroscopy (EDX) analyses were carried out for the surface imaging and elemental composition of the nanocomposite using standard procedures for sample preparation. Double-sided tape was used to adhere the dry samples onto carbon stubs. Using carbon thread evaporation under vacuum, the sample surface was coated with a thin, even layer of carbon. The Vega3 Tescan was then used to analyse this for SEM imaging and elemental composition. Fourier-transform infrared (FTIR) spectroscopic analysis was done using a PerkinElmer Spectrum 100 spectrophotometer to identify the surface functional groups of the prepared adsorbent. A 250 mg of 1% samples were prepared for analysis using the KBr pellet method. The spectra were recorded at a spectral resolution of 4 cm^{-1} in the range of 4000–400 cm^{-1}. The crystallinity of the synthesised ZnO@Ap/DETA nanocomposite was assessed by powder X-ray diffraction (XRD, Rigaku Ultima IV, Japan) with a diffractometer equipped with Cu Ka radiation ($k = 0.15406$) and a K-beta filter at 30 mA and 40 kV. These techniques confirmed the triumphant formation of ZnO@Ap/DETA and assessed its possible adsorption properties. The surface charge properties of ZnO@Ap/DETA were looked into across the pH of 1–11 using zeta potential measurements. The zeta potentials of the nanocomposites were measured using a Malvern Zetasizer nano-Z analyser with a folded capillary cell. The nanocomposite was dispersed in deionised water, and the pH was adjusted with 0.1 M NaOH or HCl solutions. This was sonicated and analysed at 25 °C with 5 runs and 200 s equilibration.

2.5 Removal of 2,4-D by adsorption

The adsorption efficiency of the ZnO@Ap/DETA nanocomposite for 2,4-D sequestration was examined through batch adsorption experiments. Key parameters, including initial 2,4-D concentration (10–150 mg L^{-1}), agitation time (2–180 min), adsorbent dosage (5–200 mg), temperature (25–45 °C), and pH,[1–11] were systematically studied. The experiments were conducted in a shaker with water at 180 rpm. Following adsorption, the remaining 2,4-D concentration was measured using a UV spectrophotometer (Agilent Cary 60, version 2.0) at 280 nm. The removal efficiency (%) was calculated using eqn (1):

$$\%\ \text{Removal} = \frac{(C_o - C_e)}{C_o} \times 100 \frac{n!}{r!(n-r)!} \frac{n!}{r!(n-r)!} \quad (1)$$

where C_o and C_e denote the initial and equilibrium 2,4-D concentrations (mg L^{-1}), respectively.

Equilibrium isotherm investigations were carried out in order to comprehend the adsorption mechanism using the Langmuir, the Freundlich, and the Temkin models. The isotherm experiments were conducted separately at 25 °C, 35 °C, and 45 °C using 5–200 mg L^{-1} initial 2,4-D concentrations at pH 3, 50 mg adsorbent dosage and 180 rpm speed for 90 minutes. These models helped assess the adsorbent's capacity, surface heterogeneity, and interaction energy. The adsorption capacity was determined using eqn (2). The nanocomposite was then tested on real wastewater samples spiked with 2,4-D to evaluate its practical applicability.

$$q_e = \frac{(C_o - C_e)V}{M} \quad (2)$$

where q_e is the adsorption capacity, V is the volume of the reaction solution, M is the mass of the adsorbent used, while C_o

and C_e are the initial and equilibrium concentrations of 2,4-D, respectively.

2.6 Optimisation of artificial neural network (ANN) for adsorption modelling

Several ANN network designs were assessed in order to create a precise prediction model for 2,4-D adsorption. The study utilised Python-based machine learning frameworks (Python v3.11.12), including Scikit-learn's MLPRegressor and TensorFlow (v2.18.0), with experimental adsorption data as inputs. Key input parameters included agitation time, temperature, adsorbent dosage, pH, and initial 2,4-D concentration, while the outputs predicted both removal efficiency (%) and adsorption capacity (q_e). Eighty per cent of the dataset was used for training, while twenty per cent was used for testing. A feed-forward neural network architecture was implemented with five input nodes, two hidden layers (initially configured with 100 neurons each), and two output nodes. Comprehensive hyperparameter optimisation was performed through grid search, evaluating the network architectures with hidden layer configurations ranging from,² to (100 100) neurons; activation functions Tanh, ReLU, and sigmoid; optimisation algorithms L-BFGS, Adam, and SGD; regularisation parameters, alpha values of 0.0001, 0.001, and 0.01; and both adaptive and constant learning rate schemes approaches. The MLPRegressor was configured with a maximum of 100 iterations, a fixed random state (seed = 42) for reproducibility, and k-fold cross-validation carried out with a fraction of 0.1. After systematic evaluation, the optimal model was selected based on performance indicators, such as coefficient of determination (R^2), mean squared error (MSE), and mean absolute error (MAE).[24,36] The finalised model was then employed to predict adsorption behaviour, with predictions validated against experimental results through error percentage analysis (eqn (3)). This rigorous optimisation process ensured the development of a robust ANN model capable of accurately simulating the adsorption dynamics of 2,4-D removal.

$$\text{Percentage error} = \frac{\text{Experimental value} - \text{Predicted value}}{\text{Experimental value}} \times 100\% \quad (3)$$

3 Results and discussions

3.1 Characterisation of ZnO@Ap/DETA nanocomposites

3.1.1 Morphology of ZnO@Ap/DETA. The morphology of the ZnO@Ap/DETA nanocomposite was thoroughly investigated using SEM and EDS. The findings are illustrated in Fig. 1(a)–(f).

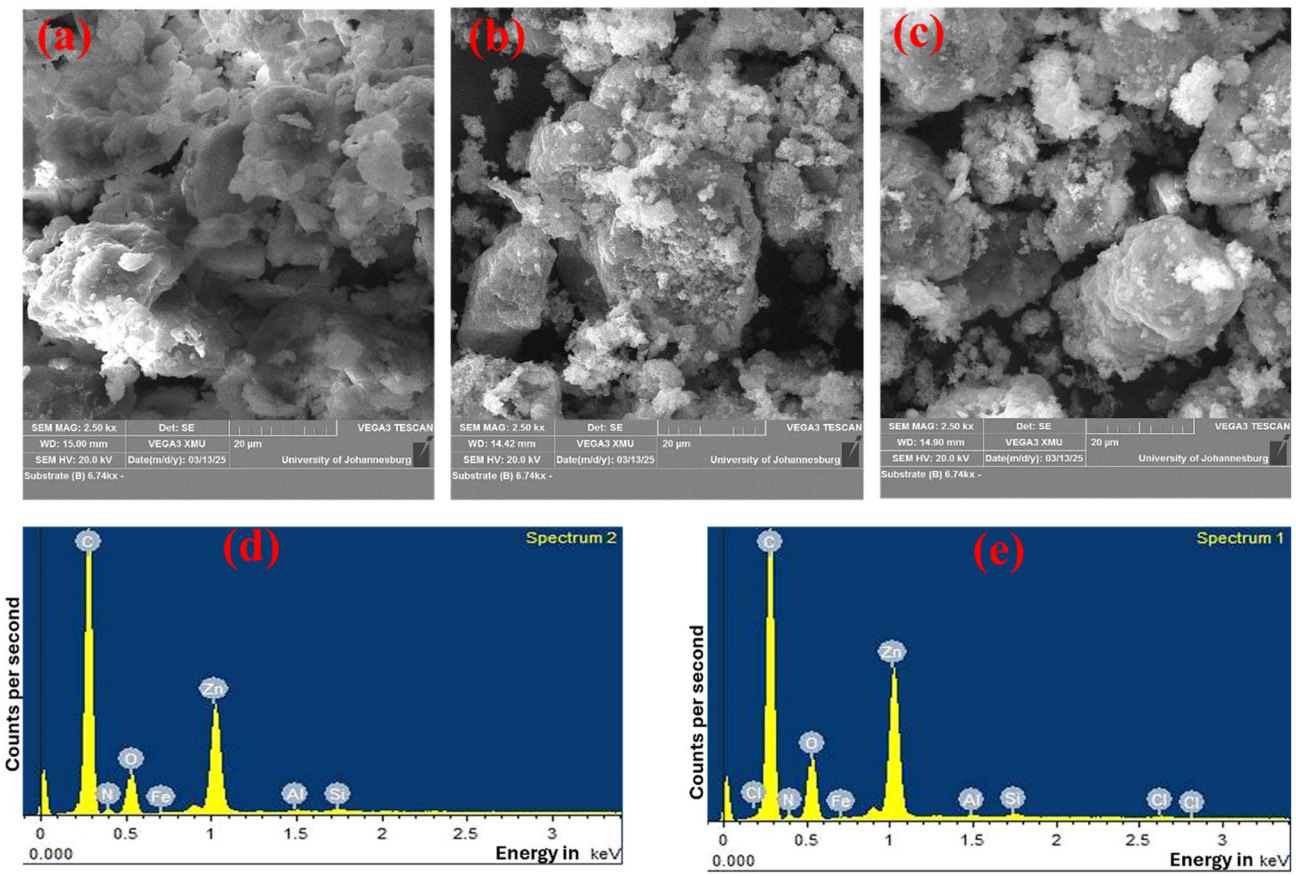

Fig. 1 SEM images of: (a) pristine Ap, (b) ZnO@Ap/DETA before adsorption, (c) ZnO@Ap/DETA after adsorption, (d) EDS analysis of ZnO@Ap/DETA before adsorption, and (e) EDS analysis of ZnO@Ap/DETA after adsorption.

At a magnification of 20 μm, Fig. 1(a) depicts the pristine apricot (AP) exhibiting large, flower-like sheet particles characterised by uneven pore distribution. In contrast, the SEM analysis of the ZnO@Ap/DETA nanocomposite (Fig. 1(b)) reveals clusters of smaller particles with a relatively uniform size distribution dispersed across the thick surfaces of the AP sheets. The SEM result of the exhausted adsorbent, presented in Fig. 1(c), indicates that some of the pores previously identified in ZnO@Ap/DETA have been occupied, implying the adherence of the pesticide 2,4-D to the surface of the ZnO@Ap/DETA.

Furthermore, the elemental composition of the ZnO@Ap/DETA nanocomposite, both prior to and following adsorption, was analysed *via* EDS, as depicted in Fig. 1(d) and (e). The presence of zinc (Zn) and nitrogen (N) was confirmed in the EDS spectrum of the ZnO@Ap/DETA nanocomposite, which was not detected in the raw AP, thereby validating the successful synthesis of ZnO using apricot shells and its subsequent modification with DETA. Also, the EDS analysis of the spent composite, shown in Fig. 1(e), indicated the existence of chlorine (Cl), demonstrating the effective removal of the pesticide 2,4-D by the composite.

Fig. 2 illustrates that the TEM image of the ZnO@Ap/DETA nanocomposite displays clusters of AP with dark hexagonal ZnO particles on the surface, further confirming the successful synthesis of the nanocomposite.

3.1.2 FTIR analysis of raw AP, ZnO@Ap/DETA before and after adsorption. The functional groups present in raw AP, as well as ZnO@Ap/DETA nanocomposite before and after adsorption, were characterised using Fourier-transform infrared (FTIR) spectroscopy. The distinct spectra are stated in Fig. 3(a). Broad bands observed at 3444 cm^{-1}, 3466 cm^{-1}, 3542 cm^{-1}, and 3399 cm^{-1} in both the pristine and modified materials are allotted to –OH stretching from lignocellulosic components of the Ap shells, interlayer water molecules, and the –NH stretching vibrations from DETA, consistent with previous reports.[37] Also, peaks appearing at 2063 cm^{-1}, 2076 cm^{-1}, and 2082 cm^{-1} across all samples are assigned to C–H stretching vibrations typical of alkyne groups. The absorption bands located at 1638 cm^{-1}, 1633 cm^{-1}, and 1637 cm^{-1} are ascribed to the stretching vibrations of carbonyl groups (C=O), indicative of ketones, aldehydes, or esters, as reported by.[38,39] The C–H bending vibrations in cellulose is shown by the band at 1384 cm^{-1}.[40] The bands observed at 1124 cm^{-1}, 1112 cm^{-1} and 1111 cm^{-1} in the raw AP, the nanocomposite and the spent adsorbent, respectively, are ascribed to C–O–C stretching vibrations in cellulose and hemicellulose, while the band at 604 cm^{-1} is assigned to C–H out-of-plane bending vibrations.[41] In the FTIR spectra of the raw Ap, characteristic peaks were detected at 2938 cm^{-1}, 1738 cm^{-1}, 1507 cm^{-1}, 1464 cm^{-1}, 1330 cm^{-1}, 1251 cm^{-1}, 1046 cm^{-1}, and 897 cm^{-1}. These bands are assigned to $-CH_2-$ methylene groups, C=O stretching from hemicellulose, C–C aromatic stretching, C–H deformation in lignin, C–O stretching in syringyl derivatives, asymmetric C–C–O aromatic stretching, C–O vibrations, and –CH deformations in cellulose and hemicellulose.[42,43] However, these characteristic peaks of the raw AP material were notably absent in the spectra of the ZnO@Ap/DETA composite, suggesting successful surface modification. Furthermore, the appearance of new peaks at 1399 cm^{-1} and 657 cm^{-1} in the composite was observed. The band at 1399 cm^{-1} is attributed to C–N stretching or CH_2 bending, while the peak at 657 cm^{-1} is assigned to Zn–O bond vibrations, confirming the incorporation of ZnO nanoparticles into the Ap and subsequent modification with DETA, consistent with previous findings on ZnO-loaded adsorbents.[44]

3.1.3 BET analysis. Nitrogen adsorption–desorption isotherms, using the BET method, were used to determine the surface area, pore volume, and pore size distribution of raw AP and the ZnO@Ap/DETA nanocomposite. The results displayed in Fig. 3(b) revealed significant structural differences between the two materials. AP exhibited a surface area of 2.0764 $m^2\ g^{-1}$, while ZnO@Ap/DETA showed a substantially higher value of

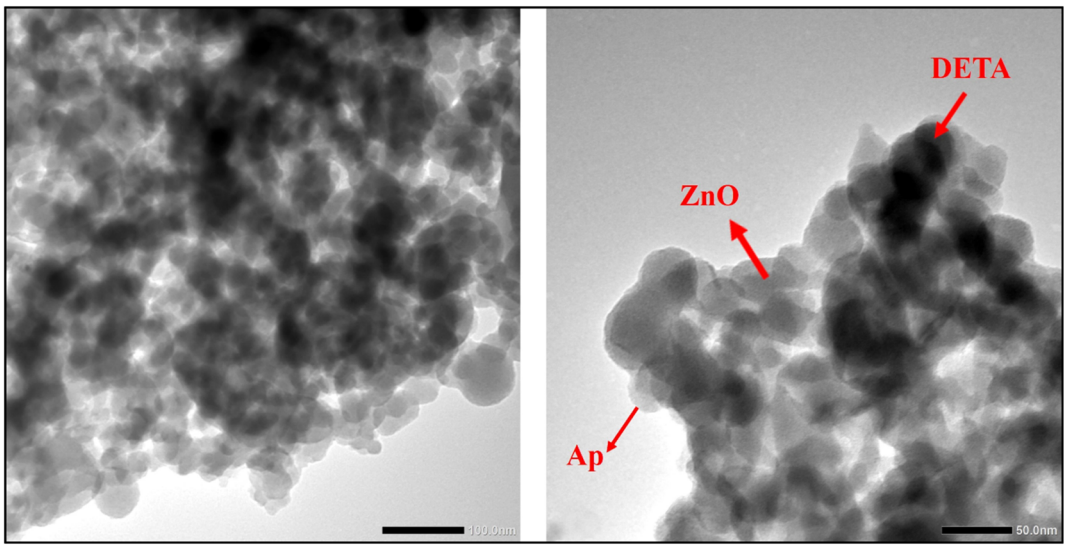

Fig. 2 TEM image of the ZnO@Ap/DETA nanocomposite.

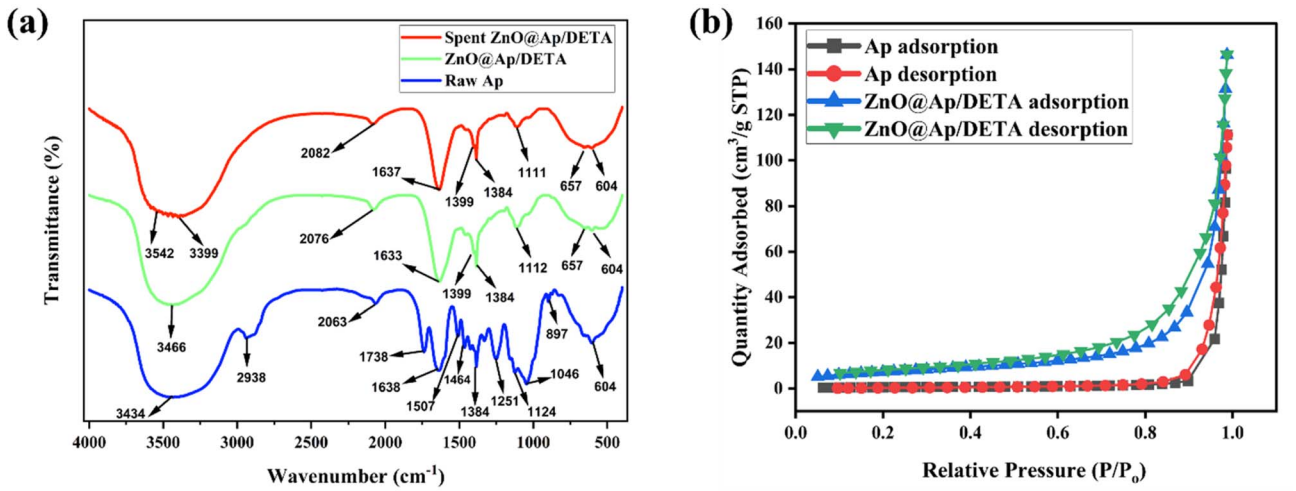

Fig. 3 (a) FTIR analysis of pristine Ap and ZnO@Ap/DETA before and after adsorption; (b) adsorption–desorption isotherm of pristine Ap and ZnO@Ap/DETA nanocomposite by BET.

26.5622 m^2 g^{-1}, an approximately 13-fold increase. The pore volume increased from 0.172 029 cm^3 g^{-1} (AP) to 0.226 217 cm^3 g^{-1} (ZnO@Ap/DETA), indicating enhanced porosity. AP had an average pore width of 331.3939 nm, whereas ZnO@Ap/DETA displayed a smaller but more uniform mesoporous structure with a pore size of 34.0659 nm. The ZnO@Ap/DETA nanocomposite demonstrated a mesoporous nature, with pore size ranging between 2 nm and 50 nm, which is favourable for adsorption applications. The significantly higher surface area and improved porosity suggest that the nanocomposite has superior adsorption capacity compared to the untreated AP material.[24]

3.1.4 XRD characterisation. The X-ray diffraction (XRD) patterns of the raw AP material, the ZnO@Ap/DETA nanocomposite, and the spent nanocomposite after adsorption are illustrated in Fig. 4(a). The raw AP exhibited broad diffraction peaks at 2θ values of 16.12°, 21.27°, and 34.60°, which are indicative of its non-crystalline, amorphous nature. These peaks are typically associated with the crystallographic planes related to cellulose I, disordered carbon structures, and amorphous carbon layers, as previously reported.[24,45,46] In contrast, the ZnO@Ap/DETA nanocomposite displayed well-defined diffraction peaks at 2θ values of 31.63°, 34.28°, 36.11°, 47.39°, 56.49°, 62.76°, 66.31°, 67.86°, 68.96°, 72.43°, and 76.87°. These peaks were indexed to the hexagonal wurtzite phase of ZnO, corresponding to the (100), (002), (101), (102), (110), (103), (200), (112), (201), (004), and (202) crystallographic planes, respectively, according to the International Centre for Diffraction Data (ICDD) card number 04-008-8199. The presence of these characteristic peaks confirms the successful incorporation of ZnO nanoparticles into the Ap/DETA.[47] Weak and broad peaks observed at 2θ values of 16.10° and 21.76° were assigned to the (110) and (002) planes of graphitic carbon structures, aligning with findings by.[48] These features further substantiate the successful synthesis of the ZnO@Ap/DETA composite. The diffraction pattern of the spent nanocomposite, recorded after the adsorption experiments, remained essentially unchanged compared to the fresh nanocomposite. This observation

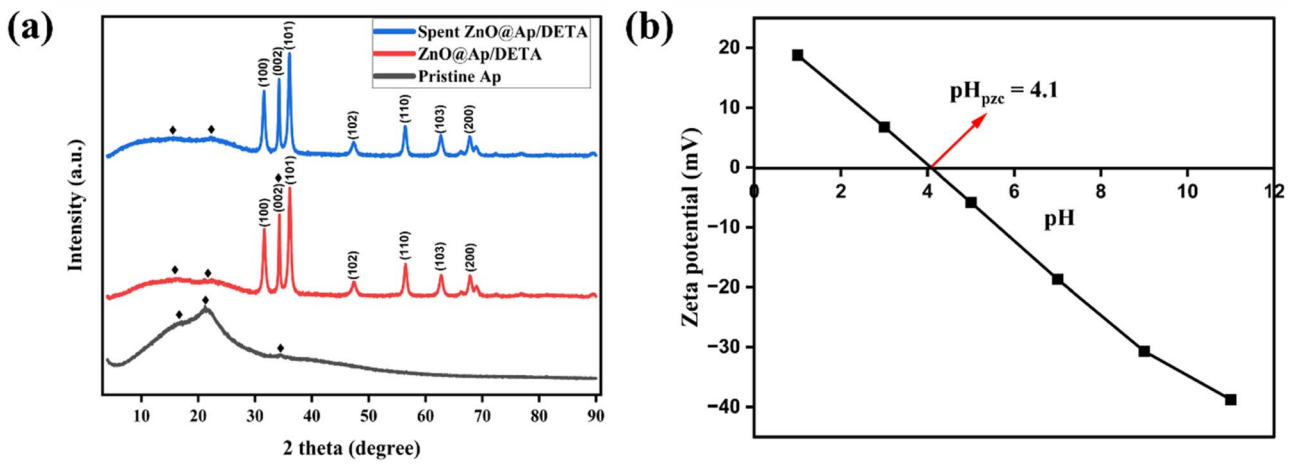

Fig. 4 (a) The XRD pattern of pristine AP, and ZnO@Ap/DETA before and after adsorption; and (b) zeta potential analysis to determine the pH point of zero charge of ZnO@Ap/DETA.

demonstrates the structural integrity and stability of the ZnO@Ap/DETA material during the adsorption process, highlighting its potential durability for practical environmental applications.

3.2 Adsorption of 2,4-D

3.2.1 Contact time study on adsorption performance. The adsorption kinetics of 2,4-D onto the ZnO@Ap/DETA nanocomposite were investigated by varying the contact time from 2 to 180 minutes under optimised conditions (25 °C, 180 rpm, pH 3, 50 mg adsorbent dose in 50 ml of 30 mg L^{-1} 2,4-D solution). As shown in Fig. 5(a), the removal efficiency exhibited rapid initial adsorption, followed by gradual attainment of equilibrium. Initially, 83.33% removal occurred within the first 30 minutes, while maximum removal efficiency (98.67%) was achieved after 90 minutes. Prolonged contact beyond 90 minutes showed no significant improvement, indicating complete occupation of available active sites. The kinetic profile demonstrates strong initial affinity between 2,4-D molecules and nanocomposite surface sites, progressive saturation of adsorption sites over time and efficient 2,4-D removal within a practical timeframe. This time-dependent behaviour is characteristic of porous adsorbents, where rapid surface adsorption precedes slower intraparticle diffusion processes. The results confirm the nanocomposite's effectiveness for rapid water treatment applications.

3.2.2 Effect of pH on adsorption efficiency. The pH of the solution plays a critical role in influencing the surface charge of ZnO@Ap/DETA, the ionisation state of 2,4-D molecules, and consequently, the adsorption capacity and efficiency of 2,4-D removal from aqueous media. Variations in pH alter the degree of protonation of the functional groups present on the adsorbent surface. At lower pH values, the surface functional groups of ZnO@Ap/DETA tend to become more protonated, enhancing their interaction with negatively charged species.[49] To examine this effect, the adsorption of 2,4-D was investigated across a pH range of 1–11 under controlled conditions, including a temperature of 25 °C, an adsorbent dosage of 50 mg, a shaking speed of 180 rpm, a contact time of 90 minutes, and an initial 2,4-D concentration of 30 mg L^{-1}. The results, as illustrated in Fig. 5(b), demonstrated a removal efficiency of 90 to 98% in

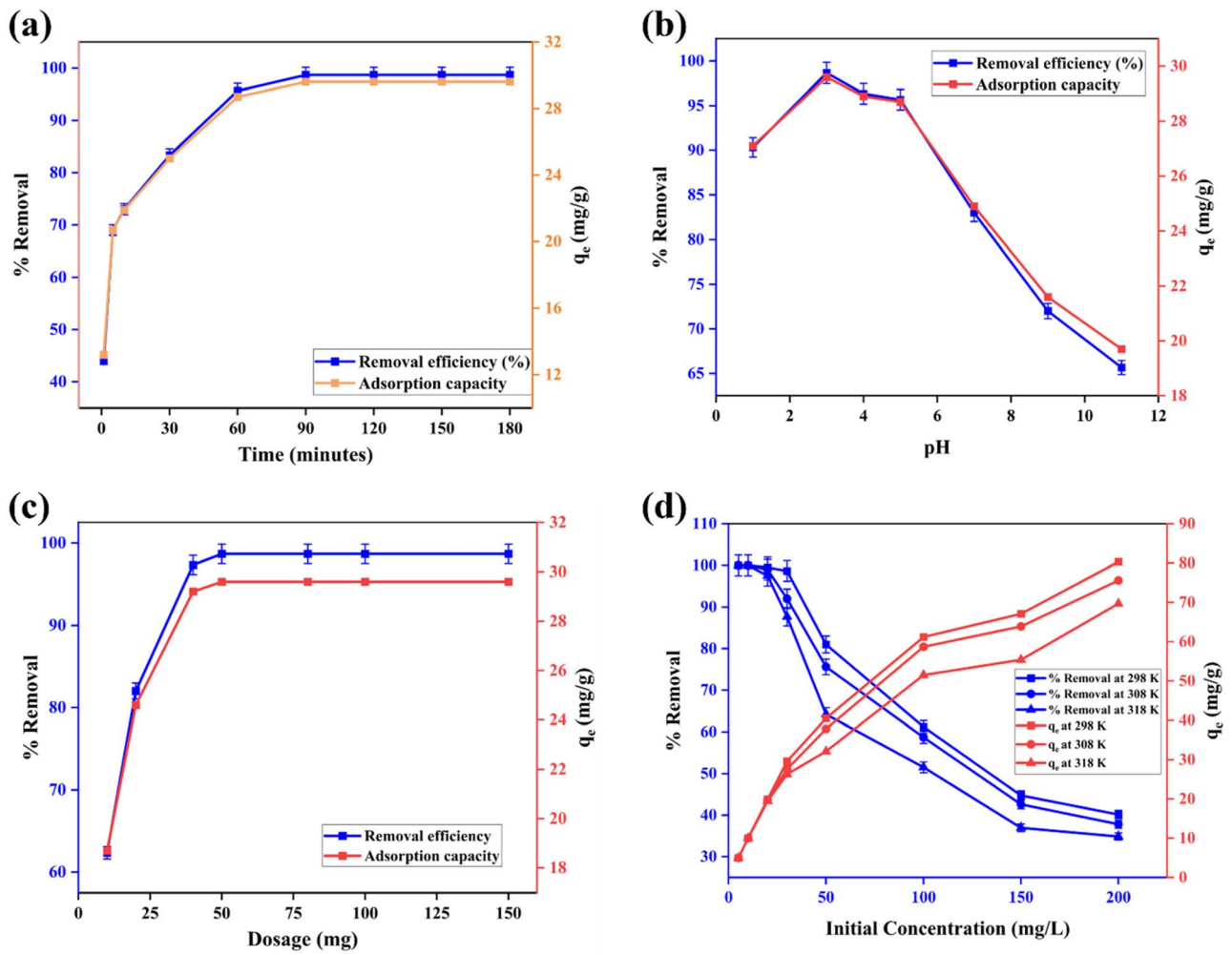

Fig. 5 Effect of (a) contact time at 25 °C, pH 3, 30 mg L^{-1} and 50 mg dosage; (b) pH at 25 °C, 30 mg L^{-1}, 50 mg dosage and 90 min; (c) dosage at 25 °C, pH 3, 30 mg L^{-1} and 90 min; (d) initial 2,4-D concentration at 25 °C, pH 3, 50 mg dosage and 90 min.

highly acidic conditions (pH 1–3), which gradually declined to 65% as the pH increased to alkaline levels (pH 5–11).

The point of zero charge (pH_{pzc}) of the adsorbent, determined through zeta potential measurements (Fig. 4(b)), was found to be 4.1. Below this pH_{pzc}, the adsorbent surface carries a positive charge, facilitating electrostatic attraction with the anionic functional groups (–COO^- and –OH) of the partly ionised 2,4-D, thereby enhancing adsorption efficiency. Conversely, at pH levels exceeding the pH_{pzc}, the surface becomes negatively charged, leading to electrostatic repulsion between the adsorbent and the ionised 2,4-D anions. 2,4-D is a weak acid that contains a carboxylic acid functional group, and its ionisation process depends on the pH of the environment medium. Above pH 4, most 2,4-D molecules are deprotonated, existing in the 2,4-D anion or the conjugate base. This is the result of the fact that the pKa of 2,4-D is about 2.7,[17] that is, above this pH the equilibrium lies in an ionised state. When the pH becomes more than 4, the surface of the adsorbent is negative and at the same time, the percentage of 2,4-D that has been deprotonated goes up hugely in level. The deprotonated form of 2,4-D is negatively charged, and this leads to electrostatic repulsion with the surface of the adsorbent,[50] thereby impacting adsorption efficiency. Resulting in reduced adsorption. Additionally, in alkaline conditions, excess hydroxide ions (OH^-) compete with 2,4-D for adsorption sites, further diminishing removal efficiency.[1] The high removal efficiency observed in acidic media can be attributed to strong electrostatic interactions between 2,4-D and ZnO@Ap/DETA, supplemented by van der Waals forces between the pesticide molecules and the diethylenetriamine (DETA) functional groups. Similar adsorption trends have been reported in previous studies,[50] reinforcing the observed pH-dependent behaviour in 2,4-D removal.

3.2.3 Dosage study on removal efficiency. The adsorption performance of ZnO@Ap/DETA nanocomposite was evaluated by varying the adsorbent dosage from 10 to 150 mg while maintaining constant conditions of pH 3, 25 °C, 180 rpm agitation, 90 min contact time, and 30 mg L^{-1} initial 2,4-D concentration in 50 mL solution. As illustrated in Fig. 5(c), the removal efficiency exhibited a dose-dependent response in which increasing the dosage from 10 mg to 50 mg enhanced removal efficiency from 62.3% to 98.7%. Further dosage increases beyond 50 mg showed negligible improvement in removal percentage. The observed trend reflects that there was greater availability of active adsorption sites at higher dosages, complete utilisation of binding sites at optimal dosage (50 mg), and possible aggregation effects at excessive dosages. This

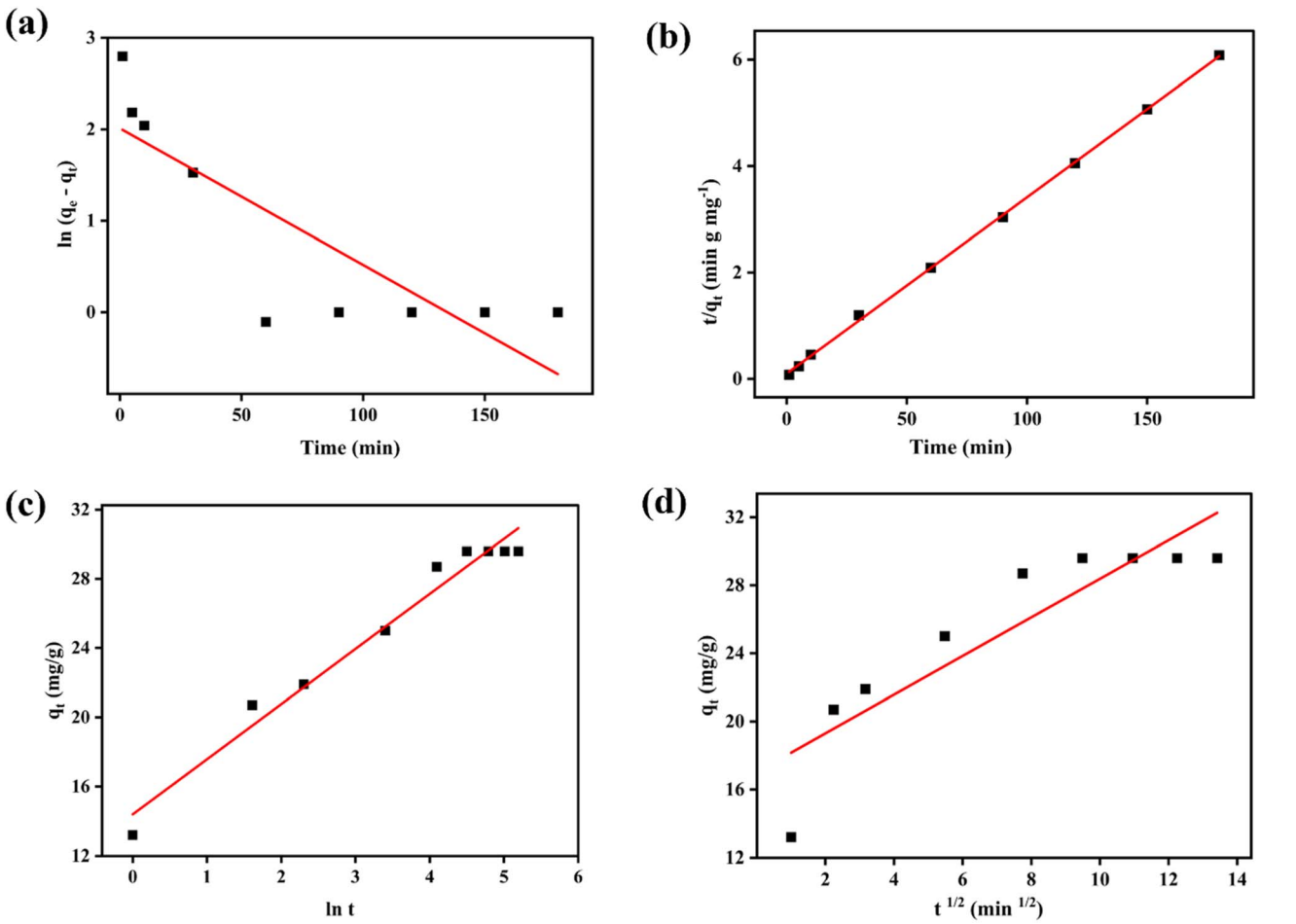

Fig. 6 Plots of the study of the (a) pseudo-first order kinetics, (b) pseudo-second order kinetic, (c) elovich kinetic, and (d) intraparticle diffusion kinetic models of the adsorption process.

shows that while higher dosages initially improved removal through increased surface area, there exists a threshold beyond which additional adsorbent provides no significant impact on removal efficiency.

3.2.4 Initial concentration and temperature study on adsorption performance. The adsorption behaviour of 2,4-D on ZnO@Ap/DETA nanocomposite was systematically studied across different initial concentrations (5–200 mg L^{-1}) and temperatures (298–318 K). The experimental results (Fig. 5(d)) revealed that the adsorption capacity reached up to 70.3 mg g^{-1} as the initial concentration was gradually increased from 5 mg L^{-1} to 200 mg L^{-1} at 298 K. However, the percentage removal efficiency decreased at higher concentrations due to rapid saturation of available active sites, increased competition among 2,4-D molecules and the limited availability of binding sites at elevated concentrations. An inverse relationship between temperature and adsorption performance was observed at 30 mg L^{-1} 2,4-D as the removal efficiency decreased from 98.6% at 298 K to 87.7% at 318 K. Similarly, the adsorption capacity declined from 70.3 mg g^{-1} to 59.7 mg g^{-1} as the temperature of the reaction system was increased from 298 K to 318 K. These findings demonstrate that optimal 2,4-D removal occurs at lower temperatures and moderate concentrations, consistent with exothermic -dominated mechanisms reported in literature.[14,51] The temperature sensitivity indicates the importance of thermal conditions in practical applications of this adsorbent system.

3.3 Kinetic analysis of 2,4-D adsorption

The adsorption mechanism of 2,4-D onto ZnO@Ap/DETA nanocomposite was investigated using four kinetic models[52–55]:

$$\ln(q_e - q_t) = \ln q_e - K_1 t \text{ (PFO)} \quad (4)$$

$$\frac{t}{q_t} = \frac{t}{q_e} + \frac{1}{K_2 {q_e}^2} \text{(PSO)} \quad (5)$$

$$Q_t = K t^{\frac{1}{2}} + C \text{(IPD)} \quad (6)$$

$$Q_t = \frac{1}{\beta}\ln(\alpha\beta) + \frac{1}{\beta}\ln\, t \text{(Elovich)} \quad (7)$$

where: PFO represents pseudo-first-order; PSO is pseudo-second-order; IPD is intra-particle diffusion; q_e and q_t are the adsorption capacities (mg g^{-1}) at equilibrium and at time t, respectively; t is the contact time (min); K_1 (min^{-1}), K_2 (g mg^{-1} min^{-1}) and K (mg g^{-1} $min^{-(1/2)}$) are the rate constants for PFO, PSO and IPD models, respectively; C (mg g^{-1}) is the boundary layer thickness constant while α (mg g^{-1} min^{-1}) is the initial adsorption rate; and β (g mg^{-1}) is the desorption constant related to chemisorption energy.

As shown in Fig. 6(b) and Table 1, the PSO model demonstrated superior fit with the highest correlation coefficient (R^2 = 0.9995), minimal sum of squared errors (SSE = 0.273462), and excellent agreement between calculated (30.21148 mg L^{-1}) and experimental (29.6 mg L^{-1}) q_e values. The PSO dominance suggests chemical interactions between 2,4-D and the nanocomposite surface, electrostatic attraction of 2,4-D to active sites of ZnO@Ap/DETA and potential involvement of valence forces through electron sharing or exchange. This kinetic behaviour aligns with previous reports of 2,4-D adsorption on various nanomaterials.[1]

Table 1 Kinetic models of the adsorption

Model	Parameter	Quantity
Pseudo-first-order		
	$q_{e(exp)}$ (mg g^{-1})	29.60
	$q_{e(cal)}$ (mg g^{-1})	7.466
	K_1 (min^{-1})	−0.01490
	R^2	0.7112
	SSE	9.898
Pseudo-second-order		
	$q_{e(exp)}$ (mg g^{-1})	29.60
	$q_{e(cal)}$ (mg g^{-1})	30.21
	K_2 (g mg^{-1} min^{-1})	0.01080
	R^2	0.9995
	SSE	0.2735
Elovich		
	α (mg g^{-1} min^{-1})	293.3
	β (g mg^{-1})	0.3142
	R^2	0.9713
Intra-particle diffusion		
	C (mg g^{-1})	17.04
	K_{diff} (mg g^{-1} $min^{-(1/2)}$)	1.135
	R^2	0.8072

3.4 Adsorption isotherm analysis

The equilibrium adsorption characteristics of 2,4-D on ZnO@Ap/DETA nanocomposite were evaluated using three fundamental isotherm models: Langmuir isotherm for monolayer adsorption, given by eqn (8); the Freundlich isotherm for heterogeneous surface, given by eqn (9); and the Temkin isotherm for the adsorption heat effects, given by eqn (10).[56–58]

$$\frac{C_e}{q_e} = \frac{K_L}{q_m} + \frac{1}{q_m}C_e \quad (8)$$

$$\ln\, q_e = \ln\, K_F + \frac{1}{n}\ln\, C_e \quad (9)$$

$$q_e = \frac{RT}{b}\ln\, K_t + \frac{RT}{b}\ln\, C_e \quad (10)$$

where: C_e is the equilibrium concentration of 2,4-D (mg L^{-1}), q_e is the equilibrium adsorption capacity (mg g^{-1}), q_m is the maximum adsorption capacity (mg g^{-1}), K_L is the Langmuir affinity constant (L mg^{-1}), R_L (dimensionless parameter) indicates adsorption favorability ($0 < R_L < 1$), K_F is the adsorption capacity indicator ((mg g^{-1})(L mg^{-1})$^{\left(\frac{1}{n}\right)}$), n^{-1} is the surface heterogeneity parameter, b is the Temkin heat of adsorption constant (J mol^{-1}), and K_t is the Temkin equilibrium binding constant (L g^{-1}), R is the gas constant (J mol^{-1} K^{-1}), and T is the absolute temperature (K).

Table 2 Isotherm parameters of the adsorption of 2,4-D onto ZnO@Ap/DETA

Models	Parameters	Temperature (K) 298	308	318
Langmuir				
	q_{max} (mg g^{-1})	76.92	72.99	66.23
	K_L (L mg^{-1})	0.3088	0.2314	0.1561
	R_L	0.1045	0.1394	0.2066
	R^2	0.9831	0.9831	0.9654
Freundlich				
	$K_F\left((\text{mg g}^{-1})(\text{L mg}^{-1})^{\left(\frac{1}{n}\right)}\right)$	18.86	14.74	12.03
	n	3.717	3.028	2.838
	R^2	0.5274	0.6656	0.7478
Temkin				
	B_T (J mol^{-1})	9.257	10.27	9.7631
	B	267.7	249.3	270.8
	K_T (L mg^{-1})	15.61	5.965	3.859
	R^2	0.7768	0.8602	0.8875

According to the fitting results (Table 2), the Langmuir model best represented the experimental data, evidenced by a high correlation coefficient ($R^2 = 0.9831$). The Freundlich and Temkin models showed comparatively lower R^2 values of 0.5274 and 0.7768, respectively. The maximum adsorption capacity of ZnO@Ap/DETA for 2,4-D, as predicted by the Langmuir model, was 76.92 mg g^{-1} at 298 K. This capacity declined with rising temperature, decreasing to 66.23 mg g^{-1} at 318 K, which remains consistent with or superior to previously reported adsorbents. The Langmuir-derived R_L values increased with temperature yet stayed within the range of 0 to 1, confirming that the adsorption process is favourable under all tested conditions.

In the Freundlich model, the ZnO@Ap/DETA exhibited strong adsorption affinity for 2,4-D, as indicated by a high K_F value of 18.86 at 298 K, which decreased as the temperature rose. The value of $n = 3.717$, being greater than 1, supports the notion of a heterogeneous surface and effective adsorbate–adsorbent interaction. Among these, the Langmuir model provided the best fit to the data, indicating a primary monolayer adsorption mechanism, a homogeneous distribution of active sites, and strong adsorbate–adsorbent interactions between 2,4-D and ZnO@Ap/DETA. These findings are consistent with earlier studies.[9] The models ranked in terms of fit quality as follows: Langmuir > Temkin > Freundlich. The ZnO@Ap/DETA material demonstrated superior performance compared to some conventional adsorbents reported in the literature, highlighting the nanocomposite's potential for water treatment applications as shown in Table 3.

3.5 Thermodynamic analysis of the adsorption of 2,4-D

The thermodynamic parameters governing the adsorption of 2,4-D onto ZnO@Ap/DETA were investigated at three different temperatures: 298 K, 308 K, and 318 K. This analysis aimed to elucidate the spontaneity, heat exchange, and disorder changes

Table 3 Comparing the adsorption capacities of various adsorbents

Adsorbent	Time (min)	q_{max} (mg g^{-1})	pH	Reference
Corn cob biochar	—	37.40	2	20
Groundnut shell char	120	3.02	—	22
Peach stone	180	~41.5	3	18
Apricot stone	180	~41.5	3	18
Orange peel	60	34.48	6	16
Wheat straw	30	1.015	4	17
Clinoptilolite modified by CTAB	<50	27	4	9
Chest nutshell	250	0.93	—	14
Balanites aegyptiaca seed shell AC	180	70.42	—	1
Tiger nut residue modified by cetylpyridinium chloride	—	79.33	3	59
Algal magnetic AC	60	60.61	2	50
ZnO@Ap/DETA	90	76.92	3	This study

associated with the adsorption process. The standard changes in Gibbs free energy (ΔG^0), enthalpy (ΔH^0), and entropy (ΔS^0), as well as the activation energy (E_a) were determined using the following thermodynamic equations[11,60–62]:

$$\Delta G^0 = -RT \ln K_L \quad (11)$$

$$\Delta G^0 = \Delta H^0 - T\Delta S^0 \quad (12)$$

$$\ln K_L = \frac{\Delta S^0}{R} - \frac{\Delta H^0}{RT} \quad (13)$$

$$E_a - \Delta H = RT \quad (14)$$

The activation energy of the adsorption was estimated from equation,[14] obtained from transition state theory. In adsorption systems, the standard enthalpy change ($\Delta H°$), usually obtained from the Van't Hoff plot, is typically considered to be an approximation of the enthalpy of activation when the thermal correction term (RT) is added to it.[62,63]

In these expressions, ΔG^0, ΔH^0, and ΔS^0 denote the standard Gibbs free energy, enthalpy, and entropy changes, respectively; R is the universal gas constant, and T is the absolute temperature. The values of ΔH^0 and ΔS^0 were calculated from the slope and intercept of the linear plot of $\ln K_L$ *versus* $\frac{1}{T}$, as depicted in SI S1.

The results for the thermodynamic parameters are shown in SI S2. The computed ΔG^0 values, which ranged from −5.185 KJ mol^{-1} to −10.66 KJ mol^{-1} across the temperature range studied, were all negative, indicating that the adsorption of 2,4-D onto ZnO@Ap/DETA is thermodynamically spontaneous. Furthermore, the negative enthalpy change ($\Delta H^0 = -92.85$ KJ mol^{-1}) confirms the exothermic nature of the process, while the negative entropy change ($\Delta S^0 = -0.2775$ KJ mol^{-1} K^{-1}) suggests a reduction in randomness at the solid–liquid interface during adsorption, potentially due to the structured arrangement of 2,4-D molecules on the adsorbent surface. These findings are in agreement with previously reported thermodynamic behaviours for similar systems, as noted in the literature.[14,51]

3.6 Mechanism of 2,4-D adsorption with ZnO@Ap/DETA nanocomposite

In order to predict the adsorption mechanism, the pH of the ZnO@Ap/DETA nanocomposite adsorbent was studied during the development of the 2, 4-D removal process. At lower pH values, where the 2,4-D molecules are less ionised, the ZnO@Ap/DETA nanocomposite adsorbent surface is predominantly positively charged, and it allows for interactions such as hydrogen bonds, π–π conjugation, van der Waals force with some of the unionised molecules of 2,4-D and electrostatic attraction with the deprotonated anions to eliminate the 2, 4-D compounds as indicated by the FTIR band shifts.[50,64,65] The shift in the FTIR bands at 3466 cm^{-1} allotted to –OH stretching from lignocellulosic components of the Ap shells, interlayer water molecules, and the –NH stretching vibrations from DETA in the nanocomposite to 3542 cm^{-1} and 3399 cm^{-1} after adsorption is indicative of the interaction of the 2,4-D with the –OH and –NH$_2$ groups on the surface of the adsorbent. Also, the movement of the peak at 2076 cm^{-1}, assigned to C–H stretching vibrations of unsaturated hydrocarbon, to 2082 cm^{-1}, and the shifting in the C=O absorption bands located at 1633 cm^{-1} to 1637 cm^{-1} in the spent adsorbent further corroborate the interaction of the C=O and C=C in the adsorption process. Thus, the –NH$_2$, –OH of ZnO@Ap/DETA nanocomposite surface and the groups on the 2,4-D pollutant, such as –COOH, and C=C created several kinds of adsorption interactions, as indicated by the FT-IR spectra band shifts at various places, as illustrated in Fig. 3(a). This kind of effect was previously shown in the adsorption of 2,4-D using a variety of adsorbents, including magnetic activated carbon nanocomposite, biochar, and magnetic hydrochar composite.[66,67] Scheme 3 shows the 2,4-D adsorption mechanism using the ZnO@Ap/DETA nanocomposite.

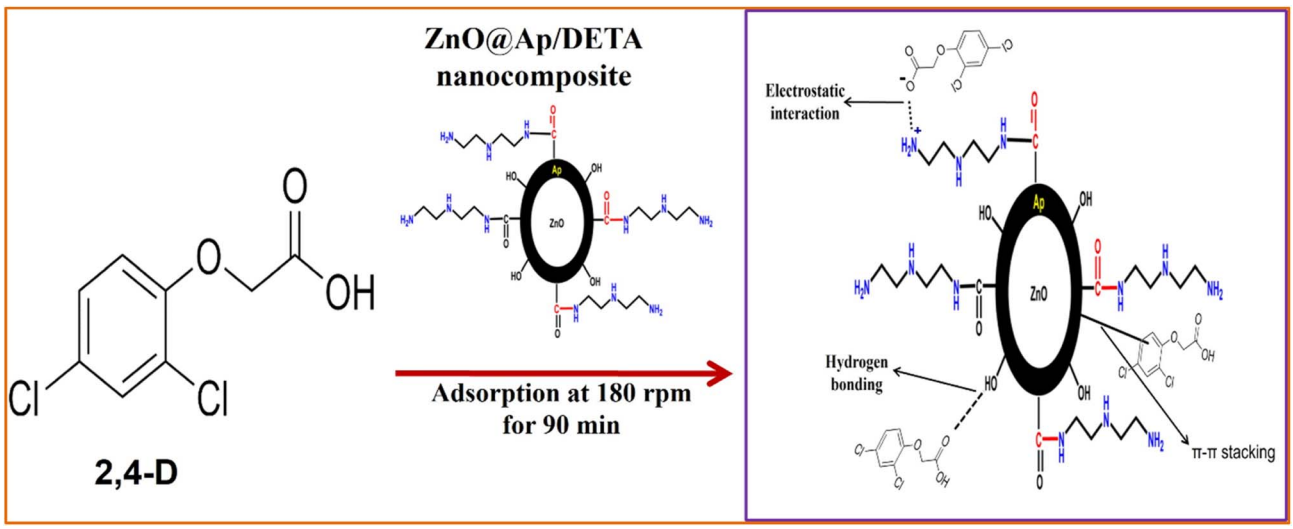

Scheme 3 The adsorption mechanism of 2,4-D with ZnO@Ap/DETA nanocomposite.

3.7 Application of ZnO@Ap/DETA for 2,4-D removal from real wastewater

The effectiveness of the ZnO@Ap/DETA nanocomposite in the removal of 2,4-D from an actual wastewater sample was assessed to determine its practical applicability. A real wastewater sample was collected from the ERWAT wastewater treatment plant in Gauteng Province of South Africa. The real wastewater sample was initially spiked with 2,4-D. The pH of the sample was determined as 3.6, and the concentration of the pesticide was measured to be 18.5 mg L^{-1} prior to treatment. Adsorption was carried out under ambient wastewater conditions at 25 °C, with an agitation speed of 180 rpm and a contact time of 90 minutes. Following treatment, the nanocomposite exhibited a removal efficiency of 85.41%, demonstrating its strong potential for effective pesticide remediation in complex environmental matrices. The slight reduction in the adsorbent's efficiency in treating a real wastewater sample compared to synthetic wastewater can be explained by the complex nature of actual effluents. In real wastewater, there are various competing ions, natural organic material, suspended solids, and colloidal species that, in addition to the target pollutant, compete with the unused sites of adsorption and, as well, may clog the pores and active sites of the adsorbent. These factors decrease the accessibility of pollutants to the active sites, leading to a relatively lower removal performance.[68,69] Synthetic wastewater, on the other hand, has only the target contaminant with controlled physicochemical conditions. Similar behaviour has also been largely reported in real wastewater treatment in complex environmental media.[70–74] These results underscore the capability of ZnO@Ap/DETA as a viable adsorbent for practical uses in the treatment of pesticide-contaminated wastewater.

3.8 Regeneration and reusability of ZnO@Ap/DETA

The reusability of the ZnO@Ap/DETA was tested. Regeneration experiments were performed to determine its ability to maintain adsorption efficiency over multiple cycles. The initial

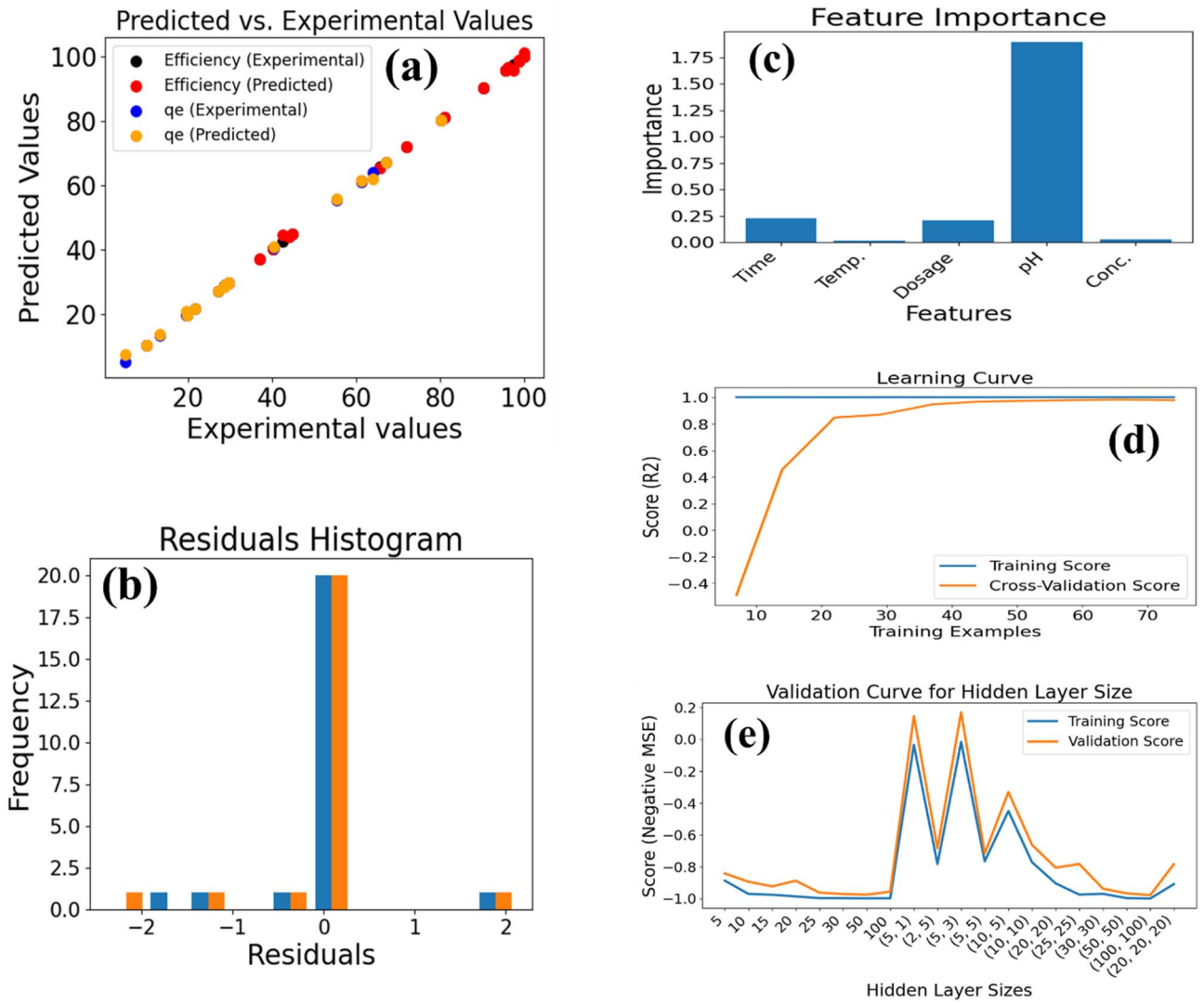

Fig. 7 (a) The plot of experimental data *versus* the ANN prediction, (b) the residuals histogram of the model, (c) the feature importance of the model, (d) the learning curve, and (e) the validation curve for the model.

adsorption was carried out with 50 mg of the adsorbent in 50 ml of a 30 mg L^{-1} 2,4-D solution at 25 °C and pH 3. This was shaken for 90 minutes at 180 rpm. After adsorption in each cycle, the nanocomposite was regenerated by stirring and washing in ethanol to remove the adsorbed 2,4-D. The material was subsequently centrifuged and dried at 60 °C for 14 hours before reusing in subsequent cycles under identical conditions of adsorption. The ZnO@Ap/DETA nanocomposite showed 70.2% adsorption efficiency for 2,4-D after five cycles of regeneration and reuse, as shown in SI S3. This result provided insights into the nanocomposite's long-term stability and potential for sustainable application in wastewater treatment.

3.9 Modelling of the adsorption efficiency and capacity

The R^2 and negative mean squared error metrics were used in the thorough grid search to determine the ideal ANN architecture. The hyperbolic tangent (tanh) activation function was used in the chosen model, and 0.0001 was assigned as the regularisation value (alpha). It used a constant learning rate and was composed of 100 neurons each in two hidden layers. With a fixed random seed of 42 to maintain consistency across multiple runs, the optimisation procedure was carried out over 100 iterations using the LBFGS method. The model was trained and assessed using the adsorption dataset, and cross-validation was carried out with a fraction of 0.1. The predictive performance of the model was evaluated by contrasting the predicted removal efficiency and qe of 2,4-D utilising ZnO@Ap/DETA with the experimental findings. Fig. 7(a) presents the graphical comparison. The model's MSE was 0.4227, and its MAE was 0.2952. Eqn (3) yielded a mean absolute percentage error of 1.5804. Excellent prediction accuracy was given by the R^2 of 0.9991. Fig. 7(b) illustrates residual analysis, which demonstrates that residuals are primarily near zero, though the distribution shows a minor asymmetry, indicating the possible presence of outliers and a non-normal error distribution. However, the overall residual pattern shows that there is little systematic bias and that the model's predictions are typically rather near to the experimental values. Based on the feature importance analysis, which is shown in Fig. 7(c), the model is mostly reliant on pH since variations in this parameter have a big impact on the predictions. Although their effects are somewhat less noticeable, other important variables influencing the prediction of the model include the agitation time and adsorbent dosage. The results of the model are not greatly impacted by temperature or the initial concentration of the pesticide.

The training and cross-validation scores are well correlated across different training set sizes, as shown by the learning curve in Fig. 7(d). These scores converge and plateau at comparable R^2 values as the dataset size grows, indicating that the model is not overfitting. At bigger sample sizes, the convergence shows consistent performance on unseen data compared to training data. This is also indicative of the fact that the model has a great potential to generalise to larger scales or unseen. The validation curve in Fig. 7(e), which looks at the effect of hidden layer size, shows that increasing model complexity generally maintains high training scores, while validation scores fluctuate and plateau for specific configurations, such as 20, 20, 20, 50, 50, and (100, 100). To balance bias and variation, the ideal complexity is approximately two hidden layers with 100 neurons each. Overall, based on the behaviour of the learning and validation curves, there are indications that the model has high generalisation capabilities without experiencing substantial overfitting or underfitting. These characteristics suggest that the model is well-fitted and demonstrates steady improvement with more data. The errors appearing randomly and unbiasedly imply that the model effectively captures underlying patterns. Thus, it has strong potential to generalise well to large and unseen data.

4 Conclusion

The development of a novel nanocomposite, diethylenetriamine functionalised zinc oxide-apricot stone shell (ZnO@Ap/DETA), has been achieved for the efficient sequestration of 2,4-D. The efficiency of removal was modelled utilising an (ANN). Characterisation of the synthesised ZnO@Ap/DETA was performed to evaluate its physicochemical properties through various instrumental methodologies. The nanocomposite exhibited a more uniform mesoporous structure having pores with an average size of 34.0659 nm and a significantly enhanced surface area of 26.5622 $m^2\ g^{-1}$, approximately 13 times greater than that of the pristine AP shells, which have 2.0764 $m^2\ g^{-1}$. The ZnO@Ap/DETA was utilised to adsorb 2,4-D from synthetic and real wastewater samples, achieving performance efficiencies of 98.6% and 85.41%, respectively, after a 90-minute shaking period at 25 °C. The data on adsorption were predominantly in adherence to the pseudo-second-order kinetic model and Langmuir isotherm, and thermodynamic investigations suggested that the process was spontaneous, favourable, and exothermic, as evidenced by a ΔH° value of −92.85 KJ mol^{-1}. To optimise the adsorption process, an ANN model was developed, comprising five input parameters, two hidden layers, and two output parameters, successfully predicting 2,4-D removal efficiency with an MAE of 0.2952, an MSE of 0.4227, and a high R^2 of 0.9991. These results highlight the potential of ZnO@Ap/DETA as a viable candidate for environmental remediation. Its effectiveness in removing 2,4-D and its ability to be regenerated for reuse offer an environmentally sustainable solution for wastewater treatment. The ANN model serves as a significant strategy for predicting and optimising adsorption parameters, thereby maximising the removal of 2,4-D and contributing to the generation of clean water.

Conflicts of interest

There are no conflicts to declare.

Data availability

Data will be made available upon request.

Supplementary information (SI): the thermodynamic data and cycles of adsorption. See DOI: https://doi.org/10.1039/d6ra00502k.

Acknowledgements

We would like to thank the National Research Foundation (NRF) and the University of Johannesburg for funding the research.

References

1 O. E. A. A. Adam and A. S. Al-Shammari, Preparation and characterization of activated carbon from Balanites aegyptiaca seed shell for the removal of 2, 4-dichlorophenoxyacetic acid herbicide from aqueous solution, *Desalin. Water Treat.*, 2023, **315**, 314–326.

2 I. Md Meftaul, K. Venkateswarlu, R. Dharmarajan, P. Annamalai and M. Megharaj, Pesticides in the urban environment: A potential threat that knocks at the door, *Sci. Total Environ.*, 2020, **11**, 134612.

3 S. Horn, R. Pieters and T. Bøhn, A first assessment of glyphosate, 2,4-D and Cry proteins in surface water of South Africa, *S. Afr. J. Sci.*, 2019, **115**, 1–7.

4 I. Engelbrecht, S. R. Horn, J. P. Giesy and R. Pieters, Quantification of Pesticides and *In Vitro* Effects of Water-Soluble Fractions of Agricultural Soils in South Africa, *Arch. Environ. Contam. Toxicol.*, 2025, **88**(2), 230–250.

5 F. Islam, J. Wang, M. A. Farooq, M. S. S. Khan, L. Xu, J. Zhu, *et al.*, Potential impact of the herbicide 2,4-dichlorophenoxyacetic acid on human and ecosystems, *Environ. Int.*, 2018, 332–351.

6 A. M. Browne and P. A. Moore, The effects of sublethal levels of 2,4-dichlorophenoxyacetic acid herbicide (2,4-D) on feeding behaviors of the crayfish O. rusticus, *Arch. Environ. Contam. Toxicol.*, 2014, **67**(2), 234–244.

7 M. E. Nault, M. D. Netherland, A. Mikulyuk, J. G. Skogerboe, T. Asplund, J. Hauxwell, *et al.*, Efficacy, selectivity, and herbicide concentrations following a whole-lake 2,4-D application targeting Eurasian watermilfoil in two adjacent northern Wisconsin lakes, *Lake Reserv. Manag.*, 2014, **30**(1), 1–10.

8 J. Gülen and S. Aslan, Adsorption of 2,4-Dichlorophenoxyacetic Acid from Aqueous Solution Using Carbonized Chest Nut as Low Cost Adsorbent: Kinetic and Thermodynamic, *Z. Phys. Chem.*, 2020, **234**(3), 461–484.

9 A. Jankowska, R. Panek, W. Franus and J. Goscianska, Tailoring Natural and Fly Ash-Based Zeolites Surfaces for Efficient 2,4-D Herbicide Adsorption: The Role of Hexadecyltrimethylammonium Bromide Modification, *Molecules*, 2024, **29**(22), 5244.

10 M. Blachnio, K. Kusmierek, A. Swiatkowski and A. Derylo-Marczewska, Waste-Based Adsorbents for the Removal of Phenoxyacetic Herbicides from Water: A Comprehensive Review, *Sustain*, 2023, **15**(23), 16516.

11 A. O. Akinola, E. Prabakaran, K. Govender and K. Pillay, Magnetically-derived pecan nut shells for the adsorptive removal of cadmium: Artificial neural network modelling and photodegradation of sulfamethoxazole using the spent sorbent, *J. Environ. Chem. Eng.*, 2025, **13**(5), 118057.

12 K. Bhattacharyya, D. Sen, A. K. Banik and S. Ganguly, Adsorptive removal of cadmium from aqueous medium-a critical review, *Phys. Chem. Earth*, 2024, **134**, 103538.

13 O. Duman, T. G. Polat, C. Ö. Diker and S. Tunç, Agar/κ-carrageenan composite hydrogel adsorbent for the removal of Methylene Blue from water, *Int. J. Biol. Macromol.*, 2020, **160**, 823–835.

14 J. Gülen and S. Aslan, Adsorption of 2,4-Dichlorophenoxyacetic Acid from Aqueous Solution Using Carbonized Chest Nut as Low Cost Adsorbent: Kinetic and Thermodynamic, *Z. Phys. Chem.*, 2020, **234**(3), 461–484.

15 S. K. Deokar and S. A. Mandavgane, Rice husk ash for fast removal of 2,4-dichlorophenoxyacetic acid from aqueous solution, *Adsorpt. Sci. Technol.*, 2015, **33**(5), 429–440.

16 V. Okumuş, K. S. Çelik, S. Özdemir, A. Dündar and E. Kılınç, Biosorption of chlorophenoxy acid herbicides from aqueous solution by using low-cost agricultural wastes, *Desalin. Water Treat.*, 2015, **56**(7), 1898–1907.

17 M. Tefera and M. Tulu, Preparation and characterization of activated carbon from wheat straw to remove 2, 4-dichlorophenoxy acetic acid from aqueous solutions, *Curr. Chem. Lett.*, 2021, **10**(3), 175–186.

18 S. Harabi, S. Guiza, J. Bedia, C. Belver and M. Bagané, Biosorption of 2,4-dichlorophenoxyacetic acid pesticide on powdered peach and apricot stones, *Int. J. Environ. Sci. Technol.*, 2024, **21**(9), 6823–6832.

19 M. I. Al-Zaben and W. K. Mekhamer, Removal of 4-chloro-2-methyl phenoxy acetic acid pesticide using coffee wastes from aqueous solution, *Arabian J. Chem.*, 2017, **10**, S1523–S1529.

20 Q. A. Binh and H. H. Nguyen, Investigation the isotherm and kinetics of adsorption mechanism of herbicide 2,4-dichlorophenoxyacetic acid (2,4-D) on corn cob biochar, *Bioresour. Technol. Rep.*, 2020, **11**, 100520.

21 Y. Liu, Y. Sun, Z. Wan, F. Jing, Z. Li, J. Chen, *et al.*, Tailored design of food waste hydrochar for efficient adsorption and catalytic degradation of refractory organic contaminant, *J. Cleaner Prod.*, 2021, **310**, 127482.

22 N. S. Trivedi, R. A. Kharkar and S. A. Mandavgane, 2,4-Dichlorophenoxyacetic acid adsorption on adsorbent prepared from groundnut shell: Effect of preparation conditions on equilibrium adsorption capacity, *Arabian J. Chem.*, 2019, **12**(8), 4541–4549.

23 Ş. Yüksel and R. Orhan, The Removal of Cr(VI) from Aqueous Solution by Activated Carbon Prepared from Apricot, Peach Stone and Almond Shell Mixture in a Fixed-Bed Column, *Arabian J. Sci. Eng.*, 2019, **44**(6), 5345–5357.

24 A. O. Akinola, E. Prabakaran, K. Govender and K. Pillay, Cetyltrimethylammonium bromide modified magnetic apricot shells for removing Congo red dye and an artificial neural network model, *New J. Chem.*, 2025, **49**(13), 5529–5544.

25 T. D. Šoštarić, M. S. Petrović, F. T. Pastor, D. R. Lončarević, J. T. Petrović, J. V. Milojković, *et al.*, Study of heavy metals

biosorption on native and alkali-treated apricot shells and its application in wastewater treatment, *J. Mol. Liq.*, 2018, **259**, 340–349.

26 I. Shaikhiev, K. Shaykhieva, S. Sverguzova, E. Fomina, Y. Vinogradenko, R. Fediuk, *et al.*, Removing Pollutants from Sewage Waters with Ground Apricot Kernel Shell Material, *Materials*, 2022, **15**(10), 3428.

27 M. Abbas, Performance of apricot stone to remove dyes from aqueous solutions-Equilibrium, kinetics, isotherms modeling and thermodynamic studies, *Mater. Today Proc.*, 2019, **31**, 437–443.

28 A. A. Mohammed and S. L. Kareem, Adsorption of tetracycline fom wastewater by using Pistachio shell coated with ZnO nanoparticles: Equilibrium, kinetic and isotherm studies, *Alexandria Eng. J.*, 2019, **58**(3), 917–928.

29 Y. Yan, B. Xiang, Y. Li and Q. Jia, Preparation and adsorption properties of diethylenetriamine-modified chitosan beads for acid dyes, *J. Appl. Polym. Sci.*, 2013, **130**(6), 4090–4098.

30 T. A. Saleh, S. O. Adio, M. Asif and H. Dafalla, Statistical analysis of phenols adsorption on diethylenetriamine-modified activated carbon, *J. Cleaner Prod.*, 2018, **182**, 960–968.

31 O. Duman, C. Özcan, T. Gürkan Polat and S. Tunç, Carbon nanotube-based magnetic and non-magnetic adsorbents for the high-efficiency removal of diquat dibromide herbicide from water: OMWCNT, OMWCNT-Fe3O4 and OMWCNT-κ-carrageenan-Fe3O4 nanocomposites, *Environ. Pollut.*, 2019, **244**, 723–732.

32 L. Mohammadi, M. Baniasadi, A. Rahdar and G. Z. Kyzas, Removal of acid dye from aqueous solutions with adsorption onto modified wheat bran – modeling with artificial neural networks, *Biointerface Res. Appl. Chem.*, 2021, **11**(6), 14044–14056.

33 N. G. Turan, B. Mesci and O. Ozgonenel, The use of artificial neural networks (ANN) for modeling of adsorption of Cu(II) from industrial leachate by pumice, *Chem. Eng. J.*, 2011, **171**(3), 1091–1097.

34 N. Daneshvar, A. R. Khataee and N. Djafarzadeh, The use of artificial neural networks (ANN) for modeling of decolorization of textile dye solution containing C. I. Basic Yellow 28 by electrocoagulation process, *J. Hazard. Mater.*, 2006, **137**(3), 1788–1795.

35 S. Ullah, M. A. Assiri, M. A. Bustam, A. G. Al-Sehemi, F. A. Abdul Kareem and A. Irfan, Equilibrium, kinetics and artificial intelligence characteristic analysis for Zn (II) ion adsorption on rice husks digested with nitric acid, *Paddy Water Environ.*, 2020, **18**(2), 455–468.

36 K. K. Ilavenil, P. Pandian and A. Kasthuri, Adsorption study of removal of lead ions using Prosopis juliflora and prediction by artificial neural network modeling, *Mater. Today Proc.*, 2023, **72**, 2344–2350.

37 Y. Ouyang, L. Zhao, M. Deng, P. Yang and G. Peng, Preparation of diethylenetriamine-functionalized thiosulfate intercalated ZnNiAl-LDHs and its removal behavior and mechanism of U(VI), *Chem. Eng. J.*, 2023, **452**, 139486.

38 A. R. Kaveeshwar, S. K. Ponnusamy, E. D. Revellame, D. D. Gang, M. E. Zappi and R. Subramaniam, Pecan shell based activated carbon for removal of iron(II) from fracking wastewater: Adsorption kinetics, isotherm and thermodynamic studies, *Process Saf. Environ. Prot.*, 2018, **114**, 107–122.

39 X. Pang, L. Sellaoui, D. Franco, G. L. Dotto, J. Georgin, A. Bajahzar, *et al.*, Adsorption of crystal violet on biomasses from pecan nutshell, para chestnut husk, araucaria bark and palm cactus: Experimental study and theoretical modeling *via* monolayer and double layer statistical physics models, *Chem. Eng. J.*, 2019, **378**, 122101.

40 M. Poletto, H. L. Ornaghi Júnior and A. J. Zattera, Native cellulose: Structure, characterization and thermal properties, *Materials*, 2014, **7**(9), 6105–6119.

41 F. Ruiz-Aquino, R. Feria-Reyes, J. G. Rutiaga-Quiñones, L. H. Robledo-Taboada and R. Gabriel-Parra, Characterization of tannin extracts derived from the bark of four tree species by HPLC and FTIR, *For. Sci. Technol.*, 2023, **19**(1), 38–46.

42 S. Sepehri, J. Javadi Moghaddam, S. Abdoli, B. Asgari Lajayer, W. Shu and G. W. Price, Application of artificial intelligence in modeling of nitrate removal process using zero-valent iron nanoparticles-loaded carboxymethyl cellulose, *Environ. Geochem. Health*, 2024, **46**(8), 262.

43 Z. Li, Y. Zhou, Q. Yin and L. Ma, Simultaneous removal of lead(II) and cadmium(II) from acidic wastewater by Fe-modified sludge biochar, *Desalin. Water Treat.*, 2024, **320**, 100716.

44 E. Altıntıg, M. Yenigun, A. Sarı, H. Altundag, M. Tuzen and T. A. Saleh, Facile synthesis of zinc oxide nanoparticles loaded activated carbon as an eco-friendly adsorbent for ultra-removal of malachite green from water, *Environ. Technol. Innovation*, 2021, **21**, 101305.

45 A. Orue, A. Eceiza and A. Arbelaiz, The use of alkali treated walnut shells as filler in plasticized poly(lactic acid) matrix composites, *Ind. Crops Prod.*, 2020, **145**, 111993.

46 Ç. S. Özdemir, H. Varliklioz and S. Yapici, Investigation of the Availability of Apricot Shell in Adsorption Equilibrium Studies, *J. Phys. Chem. Funct. Mater.*, 2018, **1**, 18–24.

47 E. Prabakaran and K. Pillay, Synthesis of N-doped ZnO nanoparticles with cabbage morphology as a catalyst for the efficient photocatalytic degradation of methylene blue under UV and visible light, *RSC Adv.*, 2019, **9**(13), 7509–7535.

48 E. Prabakaran, K. Pillay and H. Brink, Hydrothermal synthesis of magnetic-biochar nanocomposite derived from avocado peel and its performance as an adsorbent for the removal of methylene blue from wastewater, *Mater. Today Sustain.*, 2022, **18**, 100123.

49 P. Koohi, A. Rahbar-kelishami and H. Shayesteh, Efficient removal of congo red dye using Fe3O4/NiO nanocomposite: Synthesis and characterization, *Environ. Technol. Innovation*, 2021, **23**, 101559.

50 R. Vinayagam, S. Ganga, G. Murugesan, G. Rangasamy, R. Bhole, L. C. Goveas, *et al.*, 2,4-Dichlorophenoxyacetic acid (2,4-D) adsorptive removal by algal magnetic activated carbon nanocomposite, *Chemosphere*, 2023, **310**, 136883.

51 M. T. Aswani, M. Yadav, A. V. Kumar, S. Tiwari, T. Kumar and M. V. P. Kumar, Ultrasound–acid modified Merremia vitifolia biomass for the biosorption of herbicide 2,4-D from aqueous solution, *Water Sci. Technol.*, 2020, **82**(3), 468–480.

52 S. Lagergren, About the Theory of So-called Adsorption of Soluble Substances, *Sven. Vetenskapsakad. Handingarl*, 1898, **24**, 1–39.

53 G. McKay, Y. S. Ho and J. C. Y. Ng, Biosorption of Copper from Waste Waters: A Review, *Sep. Purif. Methods*, 1999, **28**(1), 87–125.

54 W. J. Weber and J. C. Morris, Closure to "Kinetics of Adsorption on Carbon from Solution.", *J. Sanit. Eng. Div.*, 1963, **89**(6), 53–55.

55 S. Y. Elovich and G. M. Zhabrova, Mechanism of the catalytic hydrogenation of ethylene on nickel. I. Kinetics of the process, *Zh. Fiz. Khim.*, 1939, **13**, 1761–1775.

56 I. Langmuir, The constitution and fundamental properties of solids and liquids. Part I. Solids, *J. Am. Chem. Soc.*, 1916, **38**(11), 2221–2295.

57 H. Freundlich, Über die Adsorption in Lösungen, *Z. Phys. Chem.*, 1907, **57U**(1), 385–470.

58 V. Temkin MJP, Recent modifications to Langmuir isotherms, *Acta Physiochim. Ussr 12*, 1940, (12), 217.

59 A. N. Kani, E. Dovi, A. A. Aryee, R. Han and L. Qu, Efficient removal of 2,4-D from solution using a novel antibacterial adsorbent based on tiger nut residues: adsorption and antibacterial study, *Environ. Sci. Pollut. Res.*, 2022, **29**(42), 64177–64191.

60 O. I. Adeiga and K. Pillay, Polyaniline decorated rooibos tea waste: An adsorbent for the removal of hexavalent chromium and its reuse as a photocatalyst for the degradation of tetracycline, *Results Eng.*, 2024, **24**, 102946.

61 O. Duman, S. Tunç and T. Gürkan Polat, Adsorptive removal of triarylmethane dye (Basic Red 9) from aqueous solution by sepiolite as effective and low-cost adsorbent, *Microporous Mesoporous Mater.*, 2015, **210**, 176–184.

62 O. A. Akinbulumo, O. J. Odejobi and E. L. Odekanle, Thermodynamics and adsorption study of the corrosion inhibition of mild steel by Euphorbia heterophylla L. extract in 1.5 M HCl, *Results Mater.*, 2020, **5**, 100074.

63 A. L. Petrou, The Free Energy of Activation as the critical factor in geochemical processes, *Chem. Geol.*, 2012, **308–309**, 50–59.

64 A. Almahri, K. S. Abou-Melha, H. A. Katouah, A. M. Albonayan, F. A. Saad, M. G. El-Desouky, *et al.*, Adsorption and removal of the harmful pesticide 2,4-dichlorophenylacetic acid from an aqueous environment *via* coffee waste biochar: Synthesis, characterization, adsorption study and optimization *via* Box-Behnken design, *J. Mol. Struct.*, 2023, **1293**, 136238.

65 L. Sellaoui, M. Bouzidi, D. S. P. Franco, A. S. Alshammari, M. Gandouzi, J. Georgin, *et al.*, Exploitation of Bauhinia forficata residual fruit powder for the adsorption of cationic dyes, *Chem. Eng. J.*, 2023, **456**, 141033.

66 G. A. Sayğılı and H. Sayğılı, Fabrication of a magnetic hydrochar composite *via* an *in situ* one-pot hydrocarbonization strategy for efficient herbicide removal, *Diam. Relat. Mater.*, 2022, **128**, 109302.

67 A. Samanth, R. Selvaraj, G. Murugesan, T. Varadavenkatesan and R. Vinayagam, Efficient adsorptive removal of 2,4-dichlorophenoxyacetic acid (2,4-D) using biomass derived magnetic activated carbon nanocomposite in synthetic and simulated agricultural runoff water, *Chemosphere*, 2024, **361**, 142513.

68 X. Li, A. Zhou, Y. Long, Y. Zhou, L. Lv, W. Zhang, *et al.*, Deep removal of phosphorus from effluent of wastewater treatment plants by nanocomposite adsorbents: a new sight on the influence of dissolved nitrogen an d the mechanisms, *Sep. Purif. Technol.*, 2026, **382**, 136047.

69 W. Srisuwan, C. Jubsilp and S. Srisorrachatr, The use of K2CO3 modified sunflower seed husks for removing of metal ions from industrial wastewater, *Chem. Eng. Trans.*, 2018, **70**, 241–246.

70 A. K. Gorelkina, I. V. Timoshchuk, N. S. Golubeva, O. V. Belyaeva, N. V. Gora and L. A. Ivanova, Adsorption of chlorine- and oxygen-containing pollutants from wastewater by activated carbons, *Theor. Appl. Ecol.*, 2022, **4**, 28–37.

71 K. D. Jayeola, D. S. Sipuka, T. I. Sebokolodi, O. V. Nkwachukwu, C. Muzenda, B. A. Koiki, *et al.*, An S-Scheme CeO2/Bi2O2S heterojunction photoanode for the photoelectrocatalytic degradation of sulfamethoxazole in synthetic and real wastewater, *Electrochim. Acta*, 2024, **507**, 145160.

72 S. Álvarez-Torrellas, J. A. Peres, V. Gil-Álvarez, G. Ovejero and J. García, Effective adsorption of non-biodegradable pharmaceuticals from hospital wastewater with different carbon materials, *Chem. Eng. J.*, 2017, **320**, 319–329.

73 B. Anil, S. Mekala, S. M. Rafi and K. Ravindhranath, Simple bio-sorbents derived from Mimusops elengi plant for the effective removal of molybdate from industrial wastewater, *Biomass Convers. Biorefinery*, 2024, **14**(6), 7939–7958.

74 S. Lakhanpal, A. Dhulia and R. Ganguly, Magnetite coated sand adsorbent for Cr(VI) removal from synthetic and pharmaceutical wastewater: adsorption isotherms and kinetics, *Arabian J. Geosci.*, 2021, **14**(12), 1180.